Mon. Not. R. Astron. Soc. **000**, 000–000 (0000) Printed 13 November 2013 (MN LATEX style file v2.2)

High-Velocity Features in Type Ia Supernova Spectra

Michael J. Childress[1,2⋆], Alexei V. Filippenko[3], Mohan Ganeshalingam[3,4], Brian P. Schmidt[1,2]

[1] *Research School of Astronomy and Astrophysics, Australian National University, Canberra, ACT 2611, Australia.*
[2] *ARC Centre of Excellence for All-sky Astrophysics (CAASTRO).*
[3] *Department of Astronomy, University of California, Berkeley, CA 94720-3411, USA.*
[4] *Lawrence Berkeley National Laboratory, Berkeley, CA 94720, USA.*

13 November 2013

ABSTRACT

We use a sample of 58 low-redshift ($z \leq 0.03$) Type Ia supernovae (SNe Ia) having well-sampled light curves and spectra near maximum light to examine the behaviour of high-velocity features (HVFs) in SN Ia spectra. We take advantage of the fact that Si II λ6355 is free of HVFs at maximum light in all SNe Ia, while HVFs are still strong in the Ca II near-infrared feature in many SNe, allowing us to quantify the strength of HVFs by comparing the structure of these two lines. We find that the average HVF strength increases with decreasing light-curve decline rate, and rapidly declining SNe Ia ($\Delta m_{15}(B) \geq 1.4$ mag) show no HVFs in their maximum-light spectra. Comparison of HVF strength to the light-curve colour of the SNe Ia in our sample shows no evidence of correlation. We find a correlation of HVF strength with the velocity of Si II λ6355 at maximum light ($v_{\rm Si}$), such that SNe Ia with lower $v_{\rm Si}$ have stronger HVFs, while those SNe Ia firmly in the "high-velocity" (i.e., $v_{\rm Si} \geq$ 12,000 km s^{-1}) subclass exhibit no HVFs in their maximum-light spectra. While $v_{\rm Si}$ and $\Delta m_{15}(B)$ show no correlation in the full sample of SNe Ia, we find a significant correlation between these quantities in the subset of SNe Ia having weak HVFs. In general, we find that slowly declining (low $\Delta m_{15}(B)$) SNe Ia, which are more luminous and more energetic than average SNe Ia, tend to produce *either* high photospheric ejecta velocities (i.e., high $v_{\rm Si}$) *or* strong HVFs at maximum light, but not both. Finally, we examine the evolution of HVF strength for a sample of SNe Ia having extensive pre-maximum spectroscopic coverage and find significant diversity of the pre-maximum HVF behaviour.

Key words: supernovae: general

1 INTRODUCTION

Type Ia supernovae (SNe Ia) remain the best standardisable candles for mapping the expansion history of the Universe and thereby constraining the nature of dark energy (Riess et al. 1998; Perlmutter et al. 1999). SN Ia luminosities appear to be governed to first order by an underlying physical mechanism which drives both the peak luminosity of the SN and the decline rate ($\Delta m_{15}(B)$) of its light curve (Phillips 1993). The observed range of $\Delta m_{15}(B)$ values is likely driven by the amount of ^{56}Ni produced in the explosion and the opacity of the ejecta (Hoeflich & Khokhlov 1996; Pinto & Eastman 2000; Mazzali et al. 2001, 2007), but the driving physical mechanism behind the realised range of these parameters remains unclear. Photometric and spectroscopic behaviour which correlates with $\Delta m_{15}(B)$ can provide important clues to, and constraints on, the physical mechanism driving the decline rate.

Much recent effort has been devoted to investigating the spectroscopic behaviour of SNe Ia, and whether features in the SN Ia spectra can elucidate the origin of SN Ia luminosity diversity. Central to these efforts has been the study of the Si II λ6355 line, the most prominently identifiable feature of SN Ia spectra. The ratio of absorption strength of the Si II λ6355 line to that of its neighbouring line Si II λ5972 has long been known to be sensitive to the SN ejecta temperature and correlates with $\Delta m_{15}(B)$ (Nugent et al. 1995; Hachinger et al. 2008). The two-dimensional parameter space defined by these lines has been proposed as a diagnostic tool for inspecting SN Ia subclasses (Benetti et al. 2005; Branch et al. 2009). More recently, the velocity of the absorption minimum of the Si II λ6355 line ($v_{\rm Si}$) in the maximum-light spectra of SNe Ia has been used to divide SNe Ia into two groups, "normal" and "high-velocity" (HV) SNe Ia, which exhibit different colour behaviour (Wang et al. 2009a) and appear to have different spatial distributions within their host galaxies (Wang et al. 2013).

Another feature in SN Ia spectra of recent interest is the frequent presence of high velocity features (HVFs) whose velocities are significantly higher (typically by a few thousand km s^{-1}) than the remainder of the normal "photospheric" ab-

⋆ E-mail:mjc@mso.anu.edu.au

sorption features. These features often appear as double-peaked absorption profiles in Si II λ6355 or the Ca II near-infrared (NIR) triplet (e.g., Gerardy et al. 2004; Mazzali et al. 2005a,b; Wang et al. 2009b; Foley et al. 2012; Childress et al. 2013), and are consistently stronger in early-time SN Ia spectra. The physical origin of the HVFs remains uncertain, but broadly speaking they must be caused by some absorbing material outside the nominal photosphere of the SN. Some suggestions for the origin of HVFs include a general density enhancement caused by swept-up (Gerardy et al. 2004) or distant (Tanaka et al. 2006) circumstellar material, an enhancement in the abundance of intermediate-mass elements (IMEs) in the outermost layers of SN Ia ejecta (see discussion in, e.g., Mazzali et al. 2005a,b; Tanaka et al. 2008), or variations in the ionization state of IMEs in the outer layers of SN Ia ejecta (Blondin et al. 2013).

In this work we focus on the relationship between the strength of HVFs in SN Ia spectra at maximum light and other properties of the SN, most importantly $\Delta m_{15}(B)$ and $v_{\rm Si}$. We exploit the fact that HVFs in the Si II λ6355 line have universally faded in all SNe Ia by maximum light but HVFs in the Ca II NIR triplet are still strong in many SNe. The Si II λ6355 line gives an independent measurement of the photospheric absorption profile, enabling a robust decoupling of photospheric and HVF absorption in the Ca II NIR triplet. We utilise a sample of 58 SNe Ia with well-sampled light curves and spectra within 5 days of maximum light from the Berkeley SN Ia Program (BSNIP; Silverman et al. 2012b) sample to show that HVFs are stronger in more-slowly declining (i.e., low $\Delta m_{15}(B)$) SNe Ia and are generally absent in HV SNe Ia.

In Section 2 we catalog the photometric and spectroscopic data in our sample, and describe the procedure for measuring the strength of HVFs in the spectra. Section 3 compares the measured HVF strengths to the light-curve properties and maximum-light $v_{\rm Si}$ values of our SN sample. In Section 4, the HVF evolution for a select few SNe Ia having extensive spectroscopic observations before maximum light is examined. We present concluding remarks in Section 5.

2 DATASET

2.1 Spectroscopic and Photometric Samples

The primary focus of this work is to measure HVFs in SN Ia spectra at maximum light, taking advantage of the fact that Si II λ6355 HVFs have faded by maximum light but Ca II NIR triplet HVFs persist for most SNe Ia. This task requires a sample of SNe Ia having well-sampled light curves so that the date of maximum light and the decline rate $\Delta m_{15}(B)$ can be accurately measured. More importantly, we require a spectroscopic sample which extends far enough into the NIR to cover the Ca II NIR triplet feature. The BSNIP (Silverman et al. 2012b) sample – collected primarily with the Kast double spectrograph (Miller & Stone 1993) on the Shane 3 m telescope at Lick Observatory – is well suited to this study, as it includes a large number of objects with both photometric and spectroscopic time series, with the spectra covering a broad range of wavelength from the UV to the near IR.

In total, we found 61 SNe Ia from the BSNIP sample having spectra within 5 days of maximum light and well-sampled light curves. Three of these have insufficient signal-to-noise ratio (S/N) in the red to reliably measure the Ca II NIR triplet absorption profile, leaving us a final sample of 58 SNe Ia. In Table 1 we report this list of SNe Ia in our dataset, the phase of the BSNIP spectrum used in the analysis, and the decline rate $\Delta m_{15}(B)$ reported in the literature.

The light curves came primarily from three sources: the Harvard CfA SN group (Hicken et al. 2009), the Carnegie Supernova Project (Contreras et al. 2010; Stritzinger et al. 2011), and the Lick Observatory Supernova Search (LOSS; Ganeshalingam et al. 2010). While LOSS naturally had light-curve coverage for almost all the SNe Ia in our sample, the light curves from CfA or CSP were sometimes better sampled or had higher S/N. LOSS and CfA report their photometry on the standard B photometric system, while CSP reports photometry in their instrument's natural system. Ganeshalingam et al. (2011) found these systems to be consistent to within about 0.03 mag, and we found here that the decline rates were similarly consistent.

When a SN had multiple sources for its light curve, we calculate the final $\Delta m_{15}(B)$ and its uncertainty as the weighted mean of values reported from all the groups. Although these three surveys used different light-curve fitters – MLCS (Riess et al. 1996; Jha et al. 2007) for CfA, SNooPy (Burns et al. 2011) for CSP, and a mean light-curve template method for LOSS – the value of $\Delta m_{15}(B)$ measured from the fitted light curve provides a consistent measure of the light-curve decline rate across all methods. Generally we found the published $\Delta m_{15}(B)$ values from different sources to agree within the quoted uncertainties.

To ensure that our sample does not suffer any major selection bias, we inspected the distribution of host-galaxy masses for those SNe Ia in our sample with host masses measured either by Neill et al. (2009) or Kelly et al. (2010). We found that 35 of our 58 SNe had host masses from those studies, with a mean and $\pm1\sigma$ mass of $\log(M_*/{\rm M}_\odot) = 10.65 \pm 0.50$ for our host-mass distribution. This compares favourably to the values of $\log(M_*/{\rm M}_\odot) = 10.60 \pm 0.64$ for Neill et al. (2009) and $\log(M_*/{\rm M}_\odot) = 10.75 \pm 0.68$ for Kelly et al. (2010). Thus, our sample has a host-mass distribution similar to that of the general sample of local SN Ia hosts. These SNe Ia arise from targeted surveys and have hosts with a higher average mass than untargeted surveys (e.g., the SDSS-SN survey; Smith et al. 2012). However, the $\Delta m_{15}(B)$ range of these SNe Ia spans the full range observed in untargeted surveys (see, e.g., Hicken et al. 2009), so we have no reason to believe any significant biases exist in our sample.

2.2 Measuring HVFs in SN Ia Spectra

Atomic transitions produce lines in SN Ia spectra which exhibit a P-Cygni profile as a result of the expanding ejecta. This profile consists of both emission and absorption components, and many overlapping lines form a "pseudo-continuum." While the profiles of individual lines may have some strong influence from line emission (see, e.g., van Rossum 2012), analysis of the apparent absorption profiles of these lines remains an important empirical tool for analysing the composition of SN Ia ejecta. In the analysis below, we quantify the strength of HVFs by examining the normalised absorption profile in the Ca II NIR triplet compared to the absorption profile of the Si II λ6355 line. Our methods are based on, and closely resemble, those we employed in our analysis of SN 2012fr in Childress et al. (2013).

We begin the inspection of a given SN Ia absorption feature by first defining the pseudo-continuum of that feature. In practice, we assign (by visual inspection) regions of the spectrum to the blue and red of the feature of interest which are smooth and featureless. A pseudo-continuum is then defined for the full absorption-profile wavelength range by fitting a line to the flux in the blue and red

Table 1. Light-Curve Properties and Spectrum Phases

SN	Phase (days)	$\Delta m_{15}(B)$ (mag)	LC Source[a]
SN1994S	0.8	1.05 ± 0.04	CfA
SN1998es	-0.9	0.98 ± 0.03	LOSS
SN1999aa	-0.5	0.94 ± 0.01	CfA, LOSS
SN1999ac	-1.5	1.18 ± 0.03	LOSS
SN2000cw	4.7	1.31 ± 0.04	LOSS
SN2000dk	0.7	1.63 ± 0.04	CfA, LOSS
SN2000dm	-2.4	1.56 ± 0.05	LOSS
SN2000dn	-1.6	1.11 ± 0.03	LOSS
SN2001br	2.0	1.35 ± 0.06	LOSS
SN2001cp	0.6	0.93 ± 0.04	CfA, LOSS
SN2001da	-1.6	1.25 ± 0.05	CfA, LOSS
SN2001eh	2.2	0.91 ± 0.01	CfA, LOSS
SN2001ep	2.5	1.34 ± 0.02	CfA, LOSS
SN2001fe	-1.0	1.03 ± 0.02	CfA
SN2002bo	-1.7	1.15 ± 0.04	LOSS
SN2002cd	0.3	0.96 ± 0.03	LOSS
SN2002eb	0.9	0.99 ± 0.03	LOSS
SN2002ef	4.0	1.04 ± 0.10	LOSS
SN2002er	-4.2	1.28 ± 0.05	LOSS
SN2002ha	-0.8	1.40 ± 0.04	CfA, LOSS
SN2002he	0.3	1.50 ± 0.03	CfA, LOSS
SN2003cq	-3.0	1.26 ± 0.05	CfA
SN2003he	2.5	0.99 ± 0.03	LOSS
SN2004gs	0.1	1.60 ± 0.02	CSP, LOSS
SN2005am	3.6	1.48 ± 0.03	CSP, LOSS
SN2005bc	1.1	1.39 ± 0.05	LOSS
SN2005cf	-1.8	1.08 ± 0.03	LOSS
SN2005de	-1.3	1.22 ± 0.03	LOSS
SN2005el	0.8	1.36 ± 0.01	CfA, CSP, LOSS
SN2005eq	-0.4	0.85 ± 0.01	CfA, CSP, LOSS
SN2005ms	-2.6	1.10 ± 0.01	CfA
SN2005na	-2.3	1.10 ± 0.01	CfA, CSP, LOSS
SN2006D	1.6	1.39 ± 0.02	CSP, LOSS
SN2006N	-1.6	1.58 ± 0.03	CfA
SN2006S	2.5	1.01 ± 0.02	CfA
SN2006X	2.0	1.05 ± 0.02	CSP, LOSS
SN2006bq	4.1	1.45 ± 0.03	CfA
SN2006bt	2.4	1.03 ± 0.01	CfA, CSP, LOSS
SN2006ef	1.7	1.33 ± 0.01	CfA, CSP, LOSS
SN2006ej	-4.0	1.35 ± 0.01	CfA, CSP, LOSS
SN2006et	3.2	1.09 ± 0.01	CfA, CSP
SN2006gt	0.9	1.66 ± 0.03	CSP
SN2006kf	-3.0	1.48 ± 0.01	CfA, CSP
SN2006sr	1.6	1.39 ± 0.04	CfA
SN2007A	-0.2	0.95 ± 0.02	CSP
SN2007F	2.6	1.04 ± 0.01	CfA
SN2007S	3.9	1.06 ± 0.01	CfA, CSP
SN2007af	-1.9	1.12 ± 0.01	CSP, LOSS
SN2007ba	4.5	1.89 ± 0.03	CSP
SN2007bc	-0.0	1.23 ± 0.01	CfA, CSP, LOSS
SN2007ci	-2.2	1.75 ± 0.03	CfA, LOSS
SN2007co	0.4	1.17 ± 0.02	CfA, LOSS
SN2007fr	-0.5	1.79 ± 0.04	LOSS
SN2007hj	-0.7	1.95 ± 0.06	LOSS
SN2008ar	2.8	1.08 ± 0.05	LOSS
SN2008ec	-0.7	1.36 ± 0.06	LOSS

[a] CfA = Hicken et al. (2009); CSP = Contreras et al. (2010), Stritzinger et al. (2011); LOSS = Ganeshalingam et al. (2010).

pseudo-continuum regions. In each panel of Figure 1, the pseudo-continuum regions are shown as the shaded grey regions, and the fitted linear pseudo-continuum profile is shown as the dashed green line.

After defining the pseudo-continuum, we normalise the absorption profile by dividing the observed flux by the fitted pseudo-continuum profile. For the Si II λ6355 line, we fit the normalised absorption profile as a single Gaussian profile in velocity space whose fit parameters are the velocity centre, velocity width, and peak absorption depth. We confirmed that the Si II λ6355 profiles of all SNe Ia in this sample are well fit at maximum light by a single Gaussian, and show no evidence for HVFs in the Si II λ6355 line.

The velocity centre, width, and absorption depth are fitted using a custom Python-based script which employs the `mpfit` package to minimise the χ^2 residuals between the observed flux and our simple parametrised line profile. To ensure that our χ^2 values are meaningful, we derive flux errors for the BSNIP spectra as follows. We first smooth the SN spectrum with a Savitszky-Golay filter, using a third-order polynomial fit over a 50 Å range. We next determine the squared residuals of the data from the smoothed data, and then calculate a running mean at each wavelength bin using a window of 20 Å. This technique provides a smooth estimator of the flux error in the data, and produced favourable fits with χ^2_ν values close to unity. The final fitted velocity centre, full width at half-maximum intensity (FWHM) velocity width, and integrated absorption area (i.e., the pseudo-equivalent width, pEW) are reported in Table 2. We also list the formal uncertainties on those quantities calculated from the covariance matrix returned by `mpfit` from our fitting routine.

Fitting the Ca II NIR triplet absorption profile is more complicated than the Si II λ6355 line. As a multiplet, the absorption profile in wavelength space for a single absorbing system in velocity space is the sum of absorption profiles for the three lines weighted by their relative strength. In the optically thin regime, these would be the Einstein B values. In the optically thick regime more typical of SN atmospheres, the lines would tend to saturate and thus have absorption strengths approaching equality (see the discussion in Childress et al. 2013, for more details). For our fits, we assume the optically thick regime and fit for two components in velocity space. We force the velocity centre and velocity width of the photospheric component of the Ca II NIR triplet to be within 10% of the values measured for the Si II λ6355 line. The HVF component of the Ca II NIR triplet feature is effectively unconstrained other than the velocity centre being forced to be higher than that of the photospheric component by 2000 km s^{-1}. Constraining the HVF velocity centre to be higher than the photospheric component was required in order to prevent the fitting routine from finding the same centre for both components, and we determined that 2000 km s^{-1} achieved successful separation of the two components while preventing the fitted HVF centre from occurring at its lower bound. The Ca II NIR triplet fit results are reported in Table 2.

In the analysis that follows, we will parametrise the strength of the HVFs by the ratio of the HVF absorption to the photospheric absorption (i.e., the pEWs). Specifically, we will call this ratio $R_{\rm HVF}$ as defined by

$$R_{\rm HVF} = \frac{\rm pEW(HVF_{CaIR})}{\rm pEW(Phot_{CaIR})}, \quad (1)$$

where the pEW values are calculated from the absorption-profile fits as described above.

For elements of discussion below, we are also interested in the

Table 2. Absorption-Profile Fit Results

SN	Si II λ6355			Photospheric Ca IR3			HVF Ca IR3		
	v (km s^{-1})	FWHM (km s^{-1})	pEW (Å)	v (km s^{-1})	FWHM (km s^{-1})	pEW (Å)	v (km s^{-1})	FWHM (km s^{-1})	pEW (Å)
SN 1994S	10190 ± 10	5650 ± 20	84 ± 1	10300 ± 70	5190 ± 140	109 ± 5	18120 ± 190	4470 ± 10	26 ± 1
SN 1995D	9930 ± 10	5630 ± 10	82 ± 1	9750 ± 20	5060 ± 10	101 ± 1	16790 ± 50	5760 ± 100	57 ± 2
SN 1995E	10520 ± 10	6750 ± 10	102 ± 1	10460 ± 20	6080 ± 10	105 ± 1	19060 ± 60	4860 ± 120	41 ± 2
SN 1998es	9930 ± 10	6100 ± 20	61 ± 1	9210 ± 90	5490 ± 10	32 ± 1	18410 ± 40	5430 ± 100	49 ± 1
SN 1999aa	10080 ± 10	5750 ± 20	58 ± 1	9820 ± 120	5180 ± 10	39 ± 1	18790 ± 140	5530 ± 310	40 ± 3
SN 1999ac	10110 ± 10	7510 ± 20	85 ± 1	10490 ± 40	6760 ± 10	81 ± 1	16950 ± 20	4470 ± 10	86 ± 1
SN 2000cw	9740 ± 10	6500 ± 20	112 ± 1	9550 ± 10	6630 ± 10	182 ± 2	16350 ± 70	5490 ± 180	98 ± 5
SN 2000dk	10440 ± 10	7370 ± 10	125 ± 1	11050 ± 10	6990 ± 40	263 ± 3	...	...	0
SN 2000dm	10740 ± 10	6510 ± 10	106 ± 1	9870 ± 40	5860 ± 10	109 ± 1	17990 ± 120	4600 ± 240	23 ± 2
SN 2000dn	10040 ± 10	6430 ± 20	101 ± 1	9550 ± 50	5790 ± 10	118 ± 1	17030 ± 110	4470 ± 240	47 ± 4
SN 2001br	12290 ± 30	8350 ± 50	90 ± 1	13060 ± 100	7520 ± 10	55 ± 1	...	...	0
SN 2001cp	10390 ± 10	5690 ± 30	81 ± 1	10190 ± 90	5120 ± 10	89 ± 2	17300 ± 250	5870 ± 550	39 ± 5
SN 2001da	11080 ± 10	7510 ± 20	117 ± 1	10590 ± 50	6760 ± 10	112 ± 1	18660 ± 40	5280 ± 80	105 ± 2
SN 2001eh	10610 ± 10	4870 ± 20	60 ± 1	10220 ± 60	4380 ± 10	64 ± 1	17870 ± 70	5120 ± 170	63 ± 4
SN 2001ep	9640 ± 10	7010 ± 10	117 ± 1	9200 ± 20	7720 ± 10	156 ± 1	15000 ± 10	7540 ± 120	97 ± 2
SN 2001fe	10720 ± 10	5670 ± 10	73 ± 1	11340 ± 50	5100 ± 10	48 ± 1	...	...	0
SN 2002bo	12860 ± 10	9090 ± 30	150 ± 1	13570 ± 20	8670 ± 70	217 ± 3	...	...	0
SN 2002cd	14720 ± 10	7350 ± 20	115 ± 1	14930 ± 20	6610 ± 10	156 ± 1	...	...	0
SN 2002eb	9960 ± 10	5450 ± 20	75 ± 1	8970 ± 10	4900 ± 10	56 ± 1	18560 ± 50	4980 ± 130	53 ± 3
SN 2002ef	11110 ± 10	6130 ± 30	106 ± 1	10220 ± 170	5560 ± 260	139 ± 8	15670 ± 470	5340 ± 650	50 ± 7
SN 2002er	11730 ± 10	6860 ± 10	107 ± 1	10950 ± 20	6280 ± 50	121 ± 1	19440 ± 20	5620 ± 40	93 ± 1
SN 2002ha	10680 ± 10	7020 ± 10	108 ± 1	10330 ± 30	6320 ± 10	113 ± 1	17350 ± 90	4470 ± 10	29 ± 1
SN 2002he	12020 ± 10	7420 ± 10	127 ± 1	11880 ± 30	7340 ± 80	175 ± 3	18830 ± 330	4470 ± 10	7 ± 1
SN 2003cq	11750 ± 20	7520 ± 40	127 ± 1	12000 ± 50	8270 ± 10	184 ± 1	...	...	0
SN 2003he	11040 ± 10	5900 ± 20	104 ± 1	10550 ± 80	5310 ± 10	145 ± 3	17010 ± 210	5370 ± 410	54 ± 6
SN 2004gs	10480 ± 10	8160 ± 20	135 ± 1	11210 ± 20	8970 ± 10	234 ± 1	...	...	0
SN 2005am	10870 ± 10	7260 ± 10	118 ± 1	11100 ± 10	7980 ± 10	202 ± 1	20000 ± 10	6710 ± 10	1 ± 1
SN 2005bc	10430 ± 10	6960 ± 10	116 ± 1	10730 ± 30	7650 ± 10	182 ± 1	17260 ± 120	5160 ± 210	29 ± 2
SN 2005cf	9900 ± 10	6120 ± 10	86 ± 1	9520 ± 50	5510 ± 10	76 ± 1	19670 ± 20	5350 ± 70	119 ± 3
SN 2005de	10110 ± 10	6460 ± 30	102 ± 1	10110 ± 50	5810 ± 10	127 ± 1	18120 ± 110	4640 ± 220	50 ± 4
SN 2005el	10190 ± 10	6310 ± 20	93 ± 1	9730 ± 30	5680 ± 10	101 ± 1	17370 ± 90	4470 ± 10	32 ± 1
SN 2005eq	9730 ± 10	5430 ± 20	55 ± 1	8880 ± 150	4880 ± 10	30 ± 1	18570 ± 80	5330 ± 200	46 ± 3
SN 2005ms	11480 ± 20	7490 ± 40	119 ± 1	10650 ± 280	6850 ± 640	98 ± 14	18550 ± 220	4470 ± 10	57 ± 5
SN 2005na	10220 ± 10	5490 ± 40	70 ± 1	9830 ± 130	4940 ± 10	44 ± 1	...	...	0
SN 2006D	10210 ± 10	6390 ± 10	100 ± 1	11750 ± 10	7040 ± 20	196 ± 1	...	...	0
SN 2006N	11110 ± 10	6910 ± 20	114 ± 1	10600 ± 50	6220 ± 10	138 ± 1	17800 ± 230	4470 ± 10	22 ± 1
SN 2006S	10430 ± 10	5170 ± 30	73 ± 1	9780 ± 110	4650 ± 10	82 ± 3	17930 ± 180	6060 ± 420	82 ± 9
SN 2006X	14890 ± 10	9750 ± 10	186 ± 1	15430 ± 10	10640 ± 10	320 ± 1	...	...	0
SN 2006bq	12910 ± 10	9010 ± 10	166 ± 1	12510 ± 20	9910 ± 10	267 ± 1	20000 ± 10	2500 ± 90	16 ± 1
SN 2006bt	10310 ± 10	8200 ± 20	130 ± 1	9280 ± 10	8680 ± 160	163 ± 5	16740 ± 50	5710 ± 130	103 ± 4
SN 2006ef	11610 ± 10	7820 ± 10	134 ± 1	10800 ± 20	7040 ± 10	169 ± 1	20270 ± 140	5220 ± 350	20 ± 2
SN 2006ej	12210 ± 10	7690 ± 10	118 ± 1	11880 ± 30	6920 ± 10	123 ± 1	18700 ± 130	4470 ± 10	15 ± 1
SN 2006et	9730 ± 10	5910 ± 20	74 ± 1	9300 ± 80	5320 ± 10	55 ± 1	17500 ± 40	5570 ± 110	94 ± 3
SN 2006gt	9660 ± 20	6910 ± 40	118 ± 1	10630 ± 10	7600 ± 10	228 ± 1	...	...	0
SN 2006kf	11070 ± 10	7400 ± 10	116 ± 1	9960 ± 10	6660 ± 10	100 ± 1	16960 ± 110	4470 ± 10	15 ± 1
SN 2006sr	11450 ± 10	7170 ± 10	116 ± 1	11130 ± 50	6820 ± 90	157 ± 3	18040 ± 320	4650 ± 520	12 ± 2
SN 2007A	10420 ± 10	5970 ± 10	88 ± 1	9850 ± 30	5370 ± 10	83 ± 1	16810 ± 60	4470 ± 10	25 ± 1
SN 2007F	10460 ± 10	5450 ± 10	86 ± 1	10720 ± 40	4900 ± 10	97 ± 1	17010 ± 180	4470 ± 10	21 ± 1
SN 2007S	10120 ± 10	5790 ± 20	66 ± 1	10000 ± 50	5210 ± 10	67 ± 1	17260 ± 50	5260 ± 90	75 ± 2
SN 2007af	10430 ± 10	6650 ± 10	106 ± 1	10370 ± 20	6230 ± 40	142 ± 1	17920 ± 60	4470 ± 10	32 ± 1
SN 2007ba	9550 ± 20	7410 ± 50	111 ± 1	10430 ± 30	6890 ± 110	255 ± 7	...	...	0
SN 2007bc	9680 ± 10	6520 ± 10	103 ± 1	9510 ± 20	5870 ± 10	135 ± 1	16670 ± 60	4060 ± 110	38 ± 2
SN 2007ci	11520 ± 10	7250 ± 20	122 ± 1	11580 ± 50	6520 ± 10	138 ± 1	17760 ± 1360	4470 ± 10	3 ± 2
SN 2007co	11210 ± 10	7270 ± 20	120 ± 1	10620 ± 40	6550 ± 10	138 ± 1	17530 ± 40	4900 ± 80	98 ± 2
SN 2007fr	10440 ± 20	6870 ± 50	112 ± 1	10810 ± 200	6230 ± 350	232 ± 14	...	...	0
SN 2007hj	11500 ± 10	8490 ± 10	147 ± 1	12130 ± 10	9340 ± 10	264 ± 1	20000 ± 10	4470 ± 10	16 ± 1
SN 2008ar	9990 ± 20	5980 ± 50	91 ± 1	8990 ± 10	5580 ± 420	92 ± 12	16870 ± 180	4470 ± 10	65 ± 3
SN 2008ec	10410 ± 10	7140 ± 10	122 ± 1	9820 ± 30	6430 ± 10	127 ± 1	16580 ± 140	4470 ± 10	17 ± 1

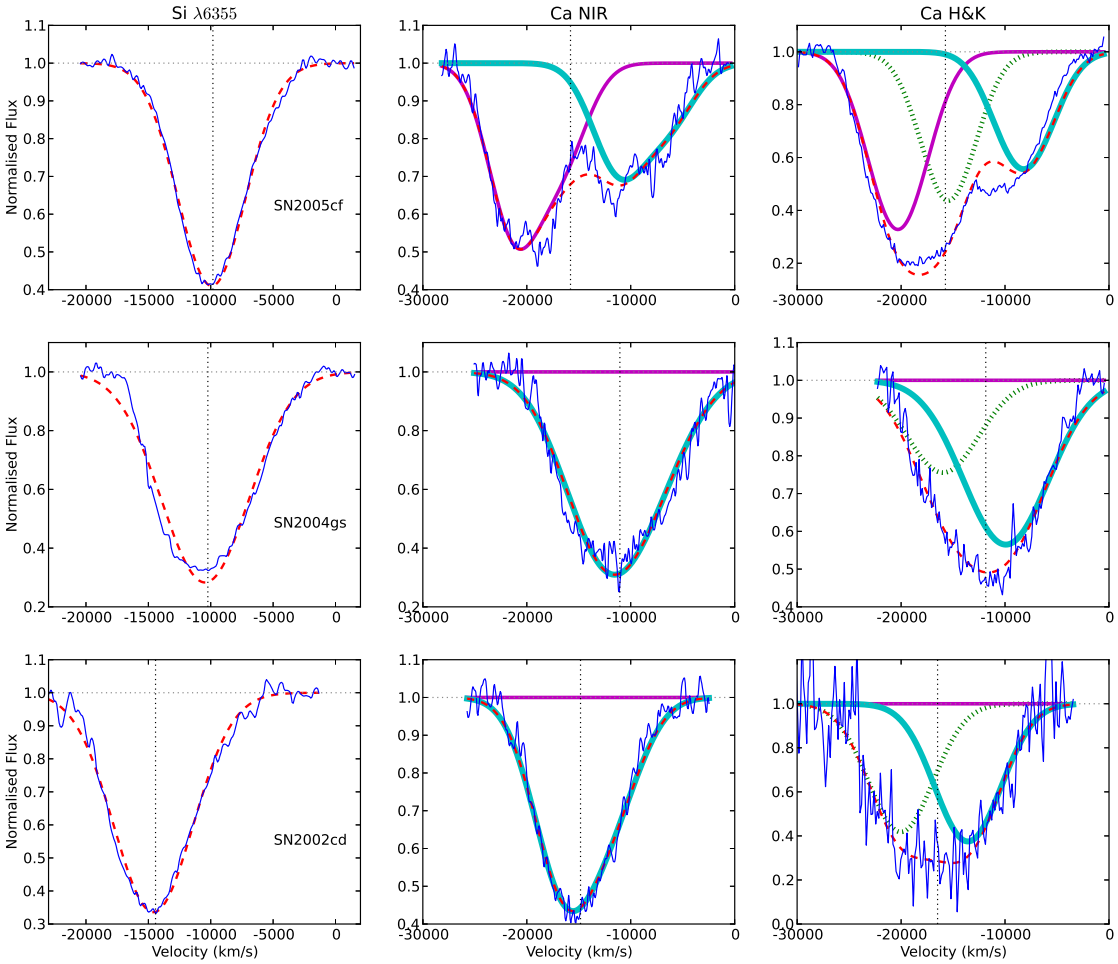

Figure 1. Absorption-profile fits for the HVF-strong and slowly declining SN 2005cf (top row); the HVF-weak and rapidly declining SN 2004gs (middle row); and the HVF-weak, slowly declining, and high-velocity (HV) SN 2002cd (bottom row). Profiles have been normalised by the fitted pseudo-continuum, with data shown in blue and the full fitted profile in dashed red. For the Ca II NIR triplet and Ca II H&K profiles (middle and right columns, respectively), the fitted photospheric absorption component is indicated as the thin magenta curve, while the fitted HVF component is the thick cyan curve. For Ca II H&K, the Si II λ3858 component is shown as the dotted green curve. The absorption-weighted velocity for each line is indicated as the vertical dotted black line in each panel (see text for details).

impact of HVFs on the Ca II H&K absorption feature. As noted by previous authors (Maguire et al. 2012; Foley 2012), this line complex is affected by the Si II λ3858 line, complicating the interpretation of HVFs in the line. As in Childress et al. (2013), we fit this line complex with three components: photospheric Ca II H&K, HVF Ca II H&K, and the Si II λ3858 line. In this work, we fixed the velocity centre and widths of these three components from the photospheric Ca II NIR triplet, HVF Ca II NIR triplet, and Si II λ6355 line-fit results, respectively, and fit only for the relative absorption strengths. Most cases resulted in the HVF Ca II H&K and Si II λ3858 line being degenerate in wavelength space, making it impossible to decompose the impact of these two components (Si II λ3858 corresponds to Ca II H&K at $v \approx 5700$ km s^{-1}, so this degeneracy is strongest when the velocity difference between photospheric and HVF Ca is in this range). Only in rare cases where the HVF Ca II H&K was at extremely high velocity (such as SN 2005cf, as shown in Figure 1) could clean separation of these two components be successfully achieved. This underscores the importance of having the clean Ca II NIR triplet absorption feature to effectively measure the velocity structure of the HVFs.

Because of this degeneracy, we do not report the results of those fits in Table 2, but we do give in Table 3 the pEW decomposition of Ca II H&K and Si II λ3858 for cases without HVFs. In this table we also report the ratio of pEW values for the Si II λ3858 line to both Ca II H&K and to Si II λ6355, with SNe Ia ordered by their $\Delta m_{15}(B)$ values. With these data we can comment on some of the trends predicted by Foley (2012). First, we find that nearly half our sample is free of HVFs, roughly consistent with the prediction by Foley (2012) that most SNe Ia should have the Ca II H&K complex free of HVFs. We also find that $\sim 48\%$ of the absorption strength in the Ca II H&K line complex appears to be caused by Si II λ3858 in the HVF-free sample. Finally, we find no strong evidence for a trend of the Si II λ3858 strength with $\Delta m_{15}(B)$, either when comparing to the true Ca II H&K absorption or to the Si II λ6355 absorption strength.

We now briefly comment on the possible effect of our choice

Table 3. Si II and Ca II H&K in no-HVF SNe Ia, ordered by $\Delta m_{15}(B)$

SN	pEW(Si) (Å)	pEW(Ca) (Å)	R_{CS} [a]	R_{Si} [b]	$\Delta m_{15}(B)$ (mag)
SN 2002cd	61	66	0.48	0.53	0.96
SN 2006bt	61	48	0.56	0.47	1.03
SN 2006X	65	91	0.42	0.35	1.05
SN 2005na	33	50	0.40	0.48	1.10
SN 2007af	62	58	0.51	0.58	1.12
SN 2002bo	70	67	0.51	0.47	1.15
SN 2007co	95	49	0.66	0.79	1.17
SN 1999ac	67	49	0.58	0.78	1.18
SN 2007bc	59	53	0.53	0.57	1.23
SN 2003cq	76	64	0.54	0.60	1.26
SN 2006ej	45	48	0.48	0.38	1.35
SN 2006D	29	74	0.28	0.29	1.39
SN 2006sr	53	54	0.49	0.46	1.39
SN 2006bq	68	63	0.52	0.41	1.45
SN 2005am	40	49	0.45	0.34	1.48
SN 2006kf	67	36	0.65	0.58	1.49
SN 2002he	58	61	0.49	0.45	1.50
SN 2000dm	51	48	0.52	0.48	1.56
SN 2006N	52	46	0.53	0.46	1.57
SN 2004gs	29	59	0.33	0.21	1.60
SN 2000dk	57	61	0.48	0.45	1.63
SN 2006gt	32	73	0.31	0.27	1.66
SN 2007fr	50	56	0.47	0.45	1.79
SN 2007ba	46	70	0.40	0.41	1.89
SN 2007hj	46	70	0.40	0.32	1.95

[a] R_{CS} = pEW(Si II λ3858) / pEW(Ca II H&K)
[b] R_{Si} = pEW(Si II λ3858) / pEW(Si II λ6355)

to constrain the photospheric Ca II NIR triplet velocity profile to be close to that of the Si II λ6355 line. For SNe Ia where the HVF in the Ca II NIR triplet is at much higher velocity (such as SN 2005cf, SN 2009ig, and SN 2012fr; see Section 4), we found that an unconstrained fit yielded the same velocity profile as when the photospheric velocity centre and width were constrained by the Si II λ6355 results. These same analyses generally found the Ca II NIR triplet photospheric velocity to be consistent with that of the Si II λ6355 velocity to within roughly 10%, so this value was used to set the velocity constraints. The difficulty arises when the HVF feature has a velocity only a few thousand km s^{-1} higher than that of the photospheric component. In these cases an unconstrained fit often yielded very narrow photospheric components and very broad HVF components, since the two components overlap in velocity space. The only way to break this degeneracy in velocity space was to impose the independent constraint obtained from the Si II λ6355 measurements. We acknowledge that the pEW decomposition of the Ca II NIR triplet profile may be imperfect owing to these constraints, but forcing a consistency between Ca II and Si II seems reasonable since we found that the velocities of these two species tend to be consistent in cases where the photospheric and HVF components cleanly separate or in cases where the lines are entirely photospheric (i.e., free of HVFs).

To provide a cross-check to our absorption-profile fits, we also desired a more model-independent measurement of the velocity profile of the absorption features. To this end, we calculated the weighted mean absorption velocity for each line as

$$\bar{v}_X = \frac{\int v \cdot a(v)\, dv}{\int a(v)\, dv}, \quad (2)$$

where $a(v)$ is the normalised absorption profile (flux divided by pseudo-continuum) in velocity space. In practice, this is calculated as the normalised absorption profile in wavelength space transformed to velocity space using the mean rest wavelength of the absorption line. For Si II λ6355 this is simply $\lambda = 6355$ Å, and for the Ca II multiplets we assume the optically thick regime which results in simply the mean wavelength of all the lines in the multiplet ($\lambda = 8567$ Å for the Ca II NIR triplet, and $\lambda = 3951$ Å for Ca II H&K). These absorption-weighted velocities are reported in Table 4. We denote the weighted mean absorption velocities for Si II λ6355, the Ca II NIR triplet, and Ca II H&K as $\bar{v}_{\rm Si}$, $\bar{v}_{\rm CI}$, and $\bar{v}_{\rm CH}$, respectively.

Finally, we revisit the issue of uncertainties in the main quantities derived in our analysis. As a representative case we discuss the uncertainty on $v_{\rm Si}$, which is typically the least uncertain quantity we measure. The formal uncertainty, as propagated from flux errors, is typically of order 10s to 100 km s^{-1}. This formal error fails to capture the uncertainty caused by non-Gaussianity of the absorption profile, and uncertainty in the true flux level of the pseudo-continuum caused by the presence of neighbouring lines. These are general unsolved problems in absorption-feature fitting for all types of SNe, and common practice is to assume the uncertainty in the absorption velocity to be a few hundred km s^{-1}, which is roughly 5% of the velocity width of the absorption profile. Thus, we consider a value of 300 km s^{-1} to be a reasonable estimate of the *systematic* uncertainty in both the fitted velocity centres of our absorption profiles and the absorption-weighted mean velocities (which suffer from the same pseudo-continuum uncertainties).

Uncertainty in the relative HVF strength ($R_{\rm HVF}$) is more difficult to quantify. Because the photospheric and HVF components frequently have nonzero overlap in velocity (and wavelength) space, the dominant source of error here would be an error in measurement of the central velocity and velocity width of the photospheric component. We found above that in cases with cleanly separable photospheric components of Si II λ6355 and the Ca II NIR triplet, these lines had consistent velocities within about 1000 km s^{-1} (which is roughly consistent with the velocity constraint placed on this line by our requirement that the photospheric Ca II NIR triplet be within 10% of the velocity of Si II λ6355, which averages about 10,000 km s^{-1}). The widths of the photospheric Ca II NIR triplet components were typically in the range 5000–8000 km s^{-1}, meaning that an error of 1000 km s^{-1} in the centre equates to perhaps 15–20% uncertainty in the pEW of that component. Since most $R_{\rm HVF}$ values are less than 1, this is the dominant source of error, so uncertainties in $R_{\rm HVF}$ should be of order 15–20% or less. Since our primary qualitative results will be demonstrated robustly with both $R_{\rm HVF}$ and the absorption-weighted velocity differences, profile-fitting uncertainties should not significantly affect our conclusions.

3 HVFS: RELATIONSHIPS TO SN Ia LIGHT CURVES AND VELOCITIES

3.1 HVFs and Light-Curve Decline Rate

Now that we have quantified the strength of the HVFs in our SN Ia sample, we inspect how the HVF strengths vary with other observable properties of the SNe. We begin with the light-curve decline rate $\Delta m_{15}(B)$, and show in Figure 2 the HVF pEW ratio $R_{\rm HVF}$ plotted versus $\Delta m_{15}(B)$ for our sample. The most apparent result of this analysis is that very rapidly declining ($\Delta m_{15}(B) \geq 1.4$

Table 4. Weighted Absorption Velocities and HVF Ratio

SN	$\bar{v}_{\rm Si}$ (km s^{-1})	$\bar{v}_{\rm CI}$ (km s^{-1})	$\bar{v}_{\rm CH}$ (km s^{-1})	$R_{\rm HVF}$
SN 1994S	9940	12110	11620	0.24 +- 0.01
SN 1995D	9770	12440	10930	0.57 +- 0.02
SN 1995E	10420	12910	12090	0.39 +- 0.02
SN 1998es	9950	15180	11580	1.50 +- 0.04
SN 1999aa	9970	14720	10250	1.03 +- 0.08
SN 1999ac	9920	14020	11280	1.06 +- 0.00
SN 2000cw	9600	11860	12710	0.54 +- 0.03
SN 2000dk	10190	11470	12050	0.00 +- 0.00
SN 2000dm	10540	11580	11960	0.21 +- 0.02
SN 2000dn	9970	11680	10790	0.40 +- 0.04
SN 2001br	12010	13070	12340	0.00 +- 0.00
SN 2001cp	10220	12500	11620	0.44 +- 0.06
SN 2001da	10960	14760	14940	0.94 +- 0.02
SN 2001eh	10570	13890	13050	0.98 +- 0.05
SN 2001ep	9370	11530	11980	0.63 +- 0.01
SN 2001fe	10470	11040	10980	0.00 +- 0.00
SN 2002bo	12500	13520	14030	0.00 +- 0.00
SN 2002cd	14420	14830	15120	0.00 +- 0.00
SN 2002eb	9810	14000	11950	0.95 +- 0.05
SN 2002ef	10930	11710	11610	0.36 +- 0.05
SN 2002er	11570	14870	14790	0.77 +- 0.01
SN 2002ha	10560	12050	11670	0.25 +- 0.01
SN 2002he	11670	12380	13010	0.04 +- 0.01
SN 2003cq	11310	12120	13950	0.00 +- 0.00
SN 2003he	10890	12610	13080	0.37 +- 0.04
SN 2004gs	10230	11040	10480	0.00 +- 0.00
SN 2005am	10760	11280	12890	0.00 +- 0.00
SN 2005bc	10160	11830	10820	0.16 +- 0.01
SN 2005cf	9830	15800	14360	1.57 +- 0.04
SN 2005de	9900	12620	13060	0.40 +- 0.03
SN 2005el	9980	11970	11720	0.32 +- 0.00
SN 2005eq	9720	14610	11550	1.52 +- 0.10
SN 2005ms	11310	13670	13010	0.58 +- 0.05
SN 2005na	9960	9700	10090	0.00 +- 0.00
SN 2006D	10050	12030	9960	0.00 +- 0.00
SN 2006N	10830	11720	12530	0.16 +- 0.01
SN 2006S	10330	14270	12790	1.00 +- 0.11
SN 2006X	14380	15170	15360	0.00 +- 0.00
SN 2006bq	12640	12920	14020	0.06 +- 0.00
SN 2006bt	9980	12570	11570	0.64 +- 0.03
SN 2006ef	11320	12000	13390	0.12 +- 0.01
SN 2006ej	11830	12690	12420	0.12 +- 0.00
SN 2006et	9830	14120	12260	1.69 +- 0.05
SN 2006gt	9430	11360	9610	0.00 +- 0.00
SN 2006kf	11040	11170	13300	0.15 +- 0.00
SN 2006sr	11230	11760	12080	0.08 +- 0.01
SN 2007A	10260	11610	10670	0.30 +- 0.00
SN 2007F	10280	12000	11040	0.22 +- 0.01
SN 2007S	10100	13930	12310	1.11 +- 0.03
SN 2007af	10070	11970	12170	0.23 +- 0.00
SN 2007ba	9210	11700	9510	0.01 +- 0.02
SN 2007bc	9480	11410	11540	0.28 +- 0.01
SN 2007ci	11230	11900	12010	0.02 +- 0.01
SN 2007co	11080	13520	13930	0.71 +- 0.02
SN 2007fr	10260	12600	10860	0.01 +- 0.04
SN 2007hj	11060	12590	11910	0.06 +- 0.00
SN 2008ar	9820	12540	13720	0.70 +- 0.03
SN 2008ec	10060	10970	11500	0.13 +- 0.01

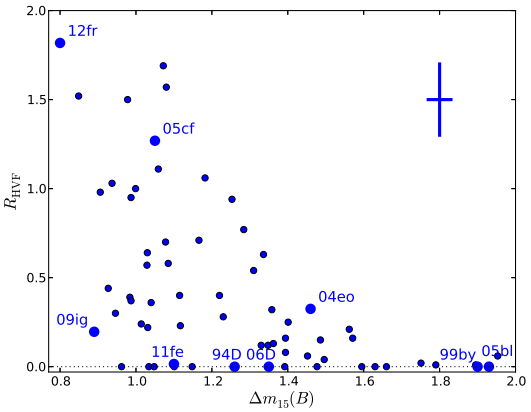

Figure 2. Ratio of absorption pseudo-equivalent width (pEW) values for the photospheric and HVF components of the Ca II NIR triplet (following the procedure outlined in Section 2.2) plotted against the light-curve decline rate $\Delta m_{15}(B)$ (compiled in Section 2.1 and Table 1). SNe Ia with spectral time series analysed in Section 4 are labeled by name and have larger symbols.

mag) SNe Ia have weak or no HVFs whatsoever. An example from this class, SN 2004gs ($\Delta m_{15}(B) = 1.60$ mag), is shown in the middle panels of Figure 1, and clearly demonstrates a similar velocity profile for the Ca II NIR triplet as for the Si II λ6355 line. Figure 2 also indicates that HVF strength tends to increase, on average, as the light-curve decline rate decreases (i.e., for the brighter SNe Ia), as can be seen for SN 2005cf ($\Delta m_{15}(B) = 1.08$ mag, shown in the top panels of Figure 1).

To confirm that the trend seen in Figure 2 is not merely an artifact of our profile-fitting procedure, we turn to the absorption-weighted velocities for the Si II λ6355 line and the Ca II NIR triplet. In the top panel of Figure 3 we show the absorption-weighted velocities for these two lines, as well as Ca II H&K, plotted against $\Delta m_{15}(B)$; the bottom panel of the same figure shows the velocity difference between the Ca II NIR triplet and the Si II λ6355 line ($\bar{v}_{\rm CI} - \bar{v}_{\rm Si}$). This figure demonstrates that the behaviour observed for the HVF absorption ratio $R_{\rm HVF}$ is observed with the same qualitative features in the model-independent measurement of mean velocity difference. Rapidly declining ($\Delta m_{15}(B) \geq 1.4$ mag) SNe Ia generally have Ca II NIR triplet profiles with similar velocities to the Si II λ6355 profile, indicating no HVF influence. Conversely, lower $\Delta m_{15}(B)$ SNe Ia tend to have Ca II NIR triplet profiles with significantly higher mean velocities than the Si II λ6355 profiles, indicating the presence of HVFs in the Ca II NIR triplet.

We note that nearly all the SNe Ia in our sample have higher absorption-weighted velocities in the Ca II NIR triplet than in the Si II λ6355 line. Even those SNe Ia which have no evidence of HVFs in the Ca II NIR triplet profile fitting show a slightly higher absorption-weighted velocity by up to $\sim$2,000 km s^{-1}. This could be caused either by very weak HVFs or by contamination from other absorption features in this range. We believe a strong candidate for this behaviour is contamination of the Ca II NIR triplet by the weak S II λ8315 line, which we identified in the late spectra of SN 2011fe and SN 2004eo (see Section 4). Though this line is weak, it presents a wavelength equivalent to the Ca II NIR triplet at a velocity of 8,800 km s^{-1}, meaning even a small amount of absorption by this line will increase the absorption-weighted Ca II

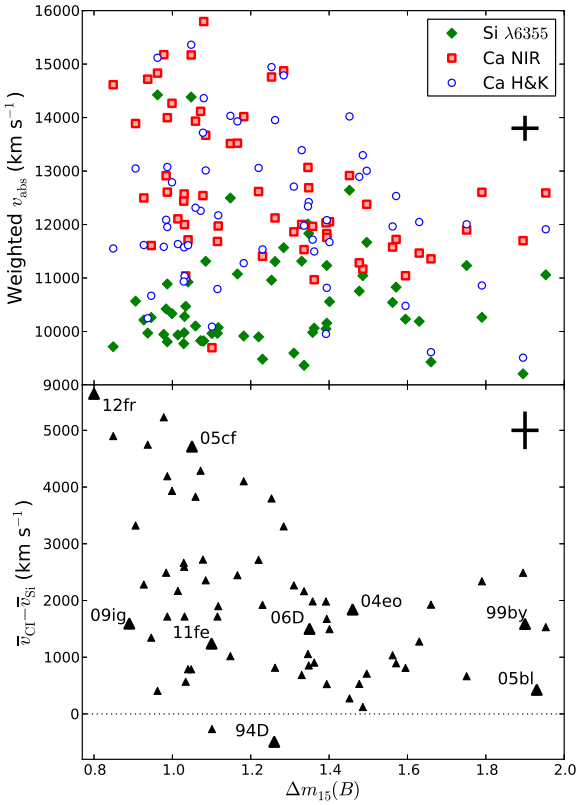

Figure 3. Top: Absorption-weighted velocities for Si II λ6355, the Ca II NIR triplet, and Ca II H&K (respectively $\bar{v}_{\rm Si}$, filled green diamonds; $\bar{v}_{\rm CI}$, shaded red squares; $\bar{v}_{\rm CH}$, open blue circles) versus light-curve decline rate $\Delta m_{15}(B)$. Bottom: Difference between $\bar{v}_{\rm CI}$ and $\bar{v}_{\rm Si}$ versus $\Delta m_{15}(B)$. SNe Ia with spectral time series analysed in Section 4 are labeled by name and have larger symbols.

NIR triplet velocity by a large amount. With sufficient S/N, this line is not erroneously fitted as a HVF component of the Ca II NIR triplet in our profile fitting, but naturally it cannot be removed from the absorption-weighted velocity calculation.

In general, we found the absorption-weighted Ca II H&K velocity ($\bar{v}_{\rm CH}$) to be equal to or higher than that of the Ca II NIR triplet. In principle, the HVF-to-photospheric pEW ratio for Ca II H&K need not be the same value as for the Ca II NIR triplet, as the Ca II H&K to Ca II NIR triplet absorption-strength ratio is temperature dependent and the HVF material could be at a different temperature than the photosphere. The Ca II lines are in the optically thick regime, meaning these temperature effects are smaller and we should expect the HVF-to-photospheric pEW ratio to be very similar for Ca II H&K and the Ca II NIR triplet. Thus subtle differences in the absorption-weighted velocities of Ca II H&K and the Ca II NIR triplet are likely due to the influence of Si II λ3858 on the Ca II H&K line complex. Quantifying this effect would likely require a model-based prediction of the Si II λ3858 absorption strength (perhaps from a $R_{\rm Si}$-based temperature estimate, see discussion in Foley 2012), which is beyond the intended scope of this work. For these reasons we focus on the Ca II NIR triplet, which offers a clean line complex for measuring HVF strength without the influence of other absorption features.

3.2 HVFs and Light-Curve Colours

Next we examine the relationship between HVF strength and the colours of SN Ia light curves. This is particularly important because it has been proposed that the absorption velocity (Foley et al. 2011; Foley & Kasen 2011) or equivalent width (Chotard et al. 2011) of the Ca II H&K line could be driven by the "intrinsic" colours (i.e., before reddening by dust) of SNe Ia. We showed above (Section 3.1) that the velocity profile of Ca II varies strongly with decline rate because of the presence of HVFs (consistent with the interpretation of the decline-rate dependence of the Ca II H&K profile proposed by Maguire et al. 2012). This raises the question of whether HVFs could be driving some (or all) of the SN Ia intrinsic colour variability.

To test this possibility, we utilise the rest-frame $(B-V)$ maximum-light colours as measured by Ganeshalingam et al. (2010) from the LOSS SN Ia light curves obtained with the 0.76 m Katzman Automatic Imaging Telescope (KAIT; Filippenko et al. 2001). In Figure 4 we plot three quantities of interest – the HVF strength ratio $R_{\rm HVF}$, the absorption-weighted mean velocities of Ca II H&K and the Ca II NIR triplet, and the absorption equivalent width of the HVF component – against the maximum-light colours of the LOSS sample. Specifically, we focus on those SNe Ia which do *not* suffer from substantial reddening by dust in their host galaxy, which we define as $(B-V) \leq 0.15$ mag, in order to gauge whether the blue edge of the distribution has some dependence on an HVF property. This colour cut is slightly more stringent than values typically employed for cosmological analyses (e.g., $c \leq 0.25$; Sullivan et al. 2011), but is roughly equivalent to the exponential reddening scale measured by Jha et al. (2007) and thus is likely to isolate SNe Ia with low reddening.

Examination of the HVF pEW ratio $R_{\rm HVF}$ or the equivalent width of the HVF absorption feature compared to the observed colours of the SNe Ia in our sample shows no obvious correlation of colour with HVF strength. Similarly, we find no clear correlation of the Ca II velocity (either Ca II H&K or the Ca II NIR triplet) with HVF strength. These efforts are unfortunately limited by the effect of foreground dust on the observed colours of the SNe Ia. To fully quantify the effect of HVFs on colours of SNe Ia, we require a larger sample of SNe Ia which are either confirmed to have no (or low) foreground reddening by dust, or whose dust reddening can be robustly measured from broad wavelength coverage including the NIR. However, our analysis indicates that HVFs do not have a strong effect on the intrinsic colours of SNe Ia.

3.3 HVFs and Silicon Velocities

Finally we consider the HVF strength compared to the absorption velocity of the Si II λ6355 line at maximum light, $v_{\rm Si}$. In Figure 5 we show the weighted absorption velocity difference ($\bar{v}_{\rm CI} - \bar{v}_{\rm Si}$) and HVF absorption ratio ($R_{\rm HVF}$) plotted against the maximum-light velocity of the Si II λ6355 line. For these plots we use the fitted velocity centre from the Si II λ6355 profile fits of Section 2.2, but found negligible differences between these values and either the weighted absorption velocity $\bar{v}_{\rm Si}$ or the velocity at the absorption minimum.

Here we found a significant dearth of HV SNe Ia with HVFs. More directly, the weighted mean velocity of the Si II λ6355 line and the Ca II NIR triplet are consistent in the maximum-light spectra of HV SNe Ia. An example of this behaviour, the HV but slowly declining SN 2002cd ($\Delta m_{15}(B) = 0.96$ mag, $v_{\rm Si} = 14600$ km s^{-1}), is shown in the lower panel of Figure 1. One could posit

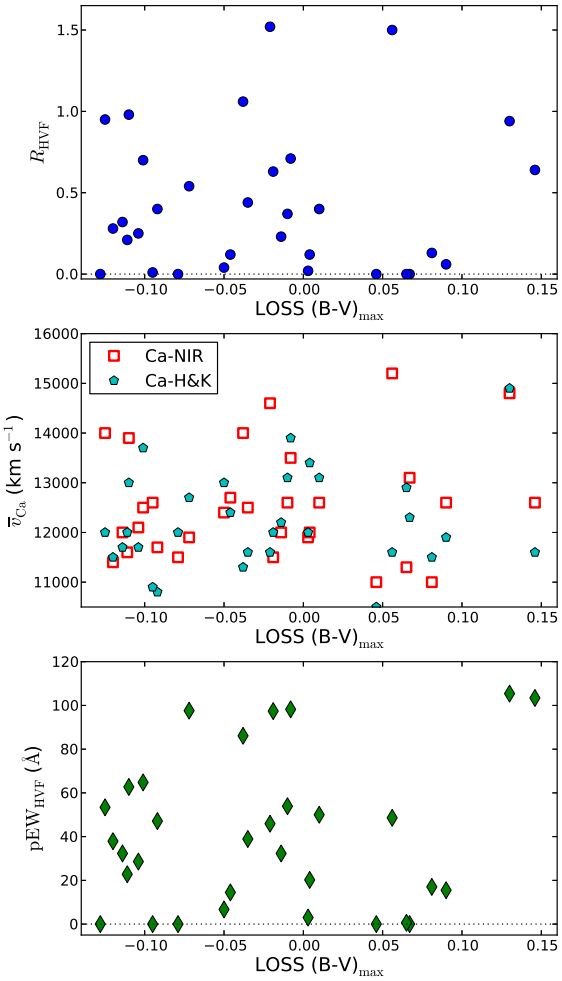

Figure 4. Top: HVF strength $R_{\rm HVF}$ versus the $(B-V)$ colour at maximum light. Middle: Absorption-weighted Ca II velocities from both the Ca II H&K (filled cyan circles) and Ca II NIR triplet (open red squares) versus colour. Bottom: Absorption equivalent width (pEW) of the HVF component of the Ca II NIR triplet versus colour.

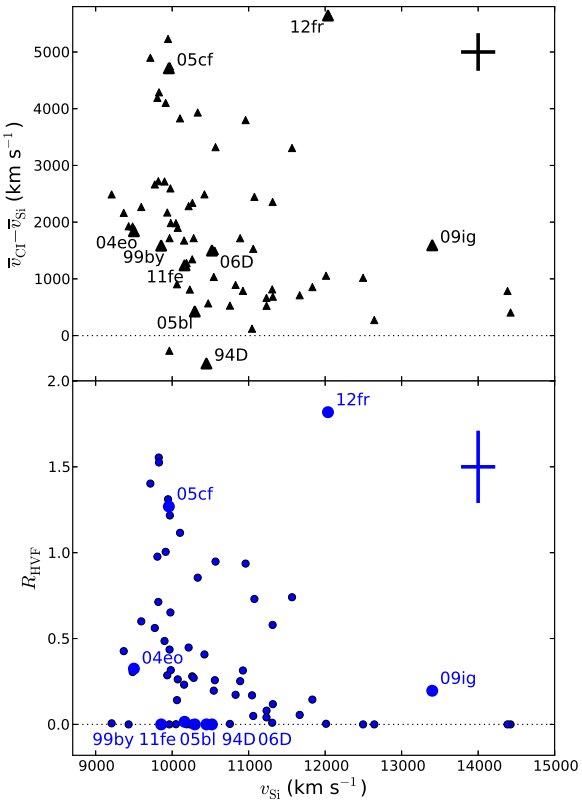

Figure 5. Top: Difference in absorption-weighted velocities ($\bar{v}_{\rm CI}-\bar{v}_{\rm Si}$) versus velocity of the Si II λ6355 line at maximum light ($v_{\rm Si}$). Bottom: HVF pEW ratio ($R_{\rm HVF}$) versus $v_{\rm Si}$. In both panels, SNe Ia with spectral time series analysed in Section 4 are labeled by name and have larger symbols.

that this behaviour may indicate that both the Si II λ6355 line and the Ca II NIR triplet are affected by HVFs, but this notion is not supported by the data for the following reasons. For SNe Ia with Si II λ6355 HVFs it has been observed that the Ca II NIR triplet HVF is much stronger than the Si II λ6355 HVF [e.g., in SN 2005cf (Garavini et al. 2007; Wang et al. 2009b), SN 2009ig (Foley et al. 2012), and SN 2012fr (Childress et al. 2013)]. As we will show in Section 4, the net result of this behaviour is that the weighted mean velocity difference ($\bar{v}_{\rm CI}-\bar{v}_{\rm Si}$) is still high when HVFs are operative, even for SNe Ia with strong Si II λ6355 HVFs. Thus, a consistent velocity between these two lines would be inconsistent with the observed behaviour of HVFs, but instead indicates a lack of HVFs in either line.

We note that the broad phase range for our sample ($-5 \leq \phi \leq 5$) could result in marginal differences between the $v_{\rm Si}$ we measure and the true $v_{\rm Si}$ at maximum light. However, even for the most rapidly evolving SNe Ia with $\dot{v}_{Si} \approx 100$ km s^{-1} day^{-1} (Benetti et al. 2005), this would yield a $v_{\rm Si}$ uncertainty of 500 km s^{-1}, which is less than 10% of the observed range of velocities ($9000 \leq v_{\rm Si} \leq 15,000$ km s^{-1}). Furthermore, the phase coverage of our sample is completely uncorrelated with $\Delta m_{15}(B)$, so we expect no bias of $v_{\rm Si}$ with $\Delta m_{15}(B)$ in our sample. Thus, we expect that our phase window has negligible effects on our conclusions.

3.4 HVFs and the Relationship Between $\Delta m_{15}(B)$ and $v_{\rm Si}$

The SN Ia expansion velocity, as tracked by $v_{\rm Si}$, shows no apparent correlation with the light-curve width $\Delta m_{15}(B)$ (see the top panel of Figure 3). For our full sample, the Pearson correlation coefficient for $v_{\rm Si}$ and $\Delta m_{15}(B)$ is $r = 0.001$, indicating no correlation. However, we found that SNe Ia with high $v_{\rm Si}$ or high $\Delta m_{15}(B)$ (i.e., rapidly declining SNe Ia) tend to be free of HVFs. We thus examine the relationship between these two quantities when splitting the sample by HVF strength.

In Figure 6 we plot $v_{\rm Si}$ versus $\Delta m_{15}(B)$ for our sample, with points colour coded by HVF strength. We define strong-HVF SNe Ia as those having $R_{\rm HVF} > 0.2$, and analogously those with $R_{\rm HVF} < 0.2$ are classified as weak-HVF SNe Ia. A striking correlation between $v_{\rm Si}$ and $\Delta m_{15}(B)$ appears evident for the weak-HVF SNe Ia. The Pearson correlation coefficient for the full weak-HVF sample is $r = 0.56$, and if we exclude the extreme outliers (SN 2001fe, SN 2005na, and SN 2011fe), this increases to $r = 0.74$. In the three-dimensional space defined by $v_{\rm Si}$, $\Delta m_{15}(B)$, and $R_{\rm HVF}$, SNe Ia appear to congregate in a nearly planar fash-

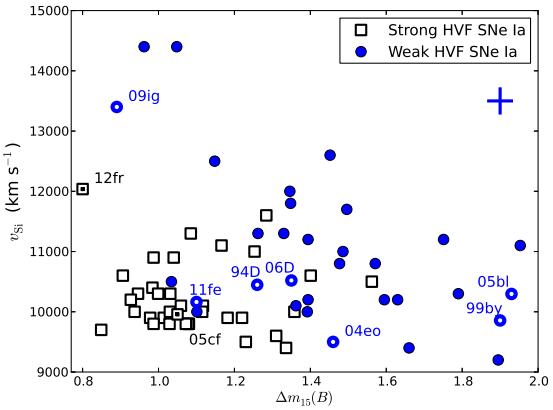

Figure 6. Si II λ6355 absorption velocity (from profile fitting) versus light-curve decline rate $\Delta m_{15}(B)$ for weak-HVF SNe Ia (filled blue circles) and strong-HVF SNe Ia (open white squares). The cutoff between weak- and strong-HVF SNe Ia is set here at $R_{\rm HVF}$= 0.2. SNe Ia with spectral time series analysed in Section 4 are labeled by name and are distinguished by a central dot.

ion. The $v_{\rm Si}$–$\Delta m_{15}(B)$ correlation observed in HVF-weak SNe Ia corresponds to where this plane intersects the $R_{\rm HVF}$= 0 surface.

While the source of this correlation remains unclear, it presents an intriguing result in the context of SN Ia explosions. SNe Ia with high $\Delta m_{15}(B)$ (fast decliners) are generally believed to be less energetic and produce less ^{56}Ni, and we see that they have both low photospheric ejecta velocities and no HVFs. Low $\Delta m_{15}(B)$ SNe Ia (slow decliners) are more energetic and produce more ^{56}Ni, and we find that they tend to produce *either* high photospheric ejecta velocities (i.e., high $v_{\rm Si}$) *or* strong HVFs, but not both.

The mechanism which sets the observed value of $v_{\rm Si}$ in a given SN Ia is a topic of rigorous study. Many detonation models – either sub-Chandra double detonations (Sim et al. 2010) or delayed detonations (e.g., Blondin et al. 2013; Seitenzahl et al. 2013) – generically result in stratified ejecta where ^{56}Ni is produced in deeper layers than IMEs like silicon. The consequence of this stratification is that $v_{\rm Si}$ effectively traces the boundary between IMEs and ^{56}Ni, so that a more energetic SN Ia which produces more ^{56}Ni naturally has a higher $v_{\rm Si}$ because the IME-^{56}Ni boundary is at larger radius. The fact that high explosion energy (i.e., low $\Delta m_{15}(B)$) is not always accompanied by high $v_{\rm Si}$ could be interpreted as an observational challenge to this picture. However, we have shown here that in cases without HVFs the observations agree qualitatively with this stratification prediction for the behaviour of $v_{\rm Si}$. Why HVF-strong SNe Ia deviate from this trend remains to be seen, but we point out that the strongest-HVF SN Ia, SN 2012fr, was shown to be highly stratified (Childress et al. 2013), so a lack of stratification seems unlikely to provide a simple explanation for this behaviour.

4 HVF EVOLUTION FOR EXTENSIVELY OBSERVED SNe Ia

Our investigation of maximum-light spectra showed an apparent dearth of HVFs in the maximum-light spectra of SNe Ia with either rapidly declining light curves or high photospheric velocities. However, it has been previously observed that HVFs are stronger at earlier epochs in SNe Ia (Mazzali et al. 2005b), so we will examine the evolution of HVFs in SNe Ia having extensive spectroscopic coverage to inspect whether HVFs are ubiquitous in the earliest spectra of SNe Ia. To perform this analysis, we downloaded spectral time series for several SNe Ia spanning a range of $\Delta m_{15}(B)$, mostly via the WISEREP (Yaron & Gal-Yam 2012) repository. In Table 5 we summarise the SN Ia sample, light-curve decline rate, and literature sources for the spectra. We note that this sample is not meant to be a comprehensive collection of all SN Ia spectral data, but instead was chosen to have broad sampling in $\Delta m_{15}(B)$ with SNe Ia having extensive spectral time series.

For the extensively observed SNe Ia analysed here, we repeat our profile-fitting procedure of Section 2.2, again taking advantage of the Si II λ6355 line to measure the photospheric velocity profile and constrain the fit of the HVF in the Ca II NIR triplet. However, some SNe Ia in this set exhibit HVFs in the Si II λ6355 line at very early epochs (though it has consistently faded by maximum light), making it more challenging to definitively identify the photospheric velocity profile. To mitigate this, we fit the Si II λ6355 line as a double-Gaussian profile in some of the earliest epochs of SN 2012fr (already presented by Childress et al. 2013), SN 2005cf, and SN 2009ig.

For all epochs of all SNe Ia, we calculate the HVF strength $R_{\rm HVF}$ in the Ca II NIR triplet, as well as the absorption-weighted velocity of Si II λ6355 ($\bar{v}_{\rm Si}$) and the Ca II NIR triplet ($\bar{v}_{\rm CI}$). In Figure 7 we plot these quantities against phase for the SNe in our sample, with colour coding ordered by $\Delta m_{15}(B)$.

The first apparent conclusion from inspection of Figure 7 is that HVF evolution does not appear to follow any universal pattern in SNe Ia. Similarly, the HVF strength at maximum light does not provide an unambiguous prediction for the pre-maximum-light behaviour of the HVFs. We briefly describe the behaviour of HVFs for each SN in our sample.

SN 2012fr. SN 2012fr is the most slowly declining ($\Delta m_{15}(B)$ = 0.80 mag) SN Ia in our sample, and also has the most extreme HVFs. As noted by Childress et al. (2013), the Ca II NIR triplet is completely dominated by HVFs during the first few days, and then the HVFs decline in strength but remain very strong overall (compared to the other SNe Ia) even through maximum light.

SN 2009ig. This slowly declining ($\Delta m_{15}(B)$ = 0.89 mag) SN Ia also begins with very strong HVFs that dominate the Ca II NIR triplet. However, the HVFs decline in strength much more rapidly than in SN 2012fr and have faded to nearly zero by about maximum light. This behaviour marks an interesting contrast to SN 2012fr (which has a similar luminosity and decline rate) because SN 2009ig is a firm member of the HV class ($v_{\rm Si}$= 13,400 km s^{-1} at maximum light; Marion et al. 2013), which we noted above tend to have no HVFs at maximum light.

SN 2005cf. Dubbed the "golden standard" SN Ia (Wang et al. 2009b), this SN Ia has a very typical decline rate and silicon velocity at maximum light. It exhibits very strong HVFs, and has perhaps the slowest HVF-strength decline rate of all SNe Ia considered here. The origin of the persistently strong HVFs (compared, especially, to SN 2011fe) is an intriguing question.

SN 2011fe. The closest and best-observed SN Ia in a generation, SN 2011fe was a prototypical example of a normal SN Ia. Its earliest epochs show no HVF in the Si II λ6355 line, but clear HVFs of modest strength in the Ca II NIR triplet. The HVF strength shows a small but statistically significant increase for the first week after the SN explosion, and then a gradual decline to zero a few days before maximum light.

SN 1994D. Considered the prototypical "core-normal" SN Ia,

Table 5. Time Series SNe Ia and their Maximum-Light Properties

SN	$\Delta m_{15}(B)$ (mag)	$v_{\rm Si}$ (km s^{-1})	$R_{\rm HVF}$	$\bar{v}_{\rm CI} - \bar{v}_{\rm Si}$ (km s^{-1})	LC Ref.	Spec. Ref.
SN 2012fr	0.80	12000	1.82	5600	1	2
SN 2009ig	0.89	13400	0.19	1600	3	3
SN 2005cf	1.05	10000	1.27	4700	4	4,5
SN 2011fe	1.10	10200	0.02	1200	6	6,7
SN 1994D	1.26	10400	0.00	-500	8	8, 9, 10
SN 2006D	1.35	10500	0.00	1500	11	12
SN 2004eo	1.46	9500	0.32	1800	13	13
SN 1999by	1.90	9900	0.00	1600	14	14
SN 2005bl	1.93	10300	0.00	400	15	15

References: (1) Contreras et al., 2013, in preparation; (2) Childress et al. (2013); (3) Foley et al. (2012); (4) Wang et al. (2009b); (5) Garavini et al. (2007); (6) Pereira et al. (2013); (7) Parrent et al. (2012); (8) Patat et al. (1996); (9) CfA (Blondin et al. 2012); (10) BSNIP (Silverman et al. 2012b); (11) Hicken et al. (2009); (12) Thomas et al. (2007); (13) Pastorello et al. (2007); (14) Garnavich et al. (2004); (15) Taubenberger et al. (2008).

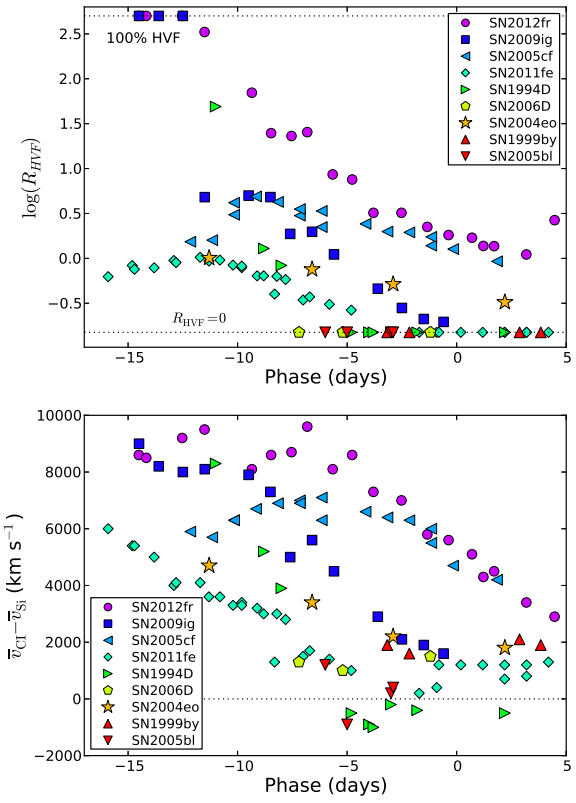

Figure 7. Top: HVF pEW ratio ($R_{\rm HVF}$) versus phase for a sample of well-observed SNe Ia. Bottom: Difference in absorption-weighted velocities ($\bar{v}_{\rm CI} - \bar{v}_{\rm Si}$) versus phase for the same sample.

SN 1994D shows strong HVFs in its first few spectroscopic epochs, which decline in strength at a rate more rapid than that of any other SN in our sample. SN 1994D has a normal $v_{\rm Si}$ at maximum light ($\sim$ 10,700 km s^{-1}; Silverman et al. 2012a), so this rapid HVF decline is apparently not associated with HV behaviour.

SN 2006D. This SN Ia showed some of the strongest absorption by unburned carbon ever observed in a SN Ia (Thomas et al. 2007), and has a modestly rapid decline rate ($\Delta m_{15}(B) = 1.35$ mag). Its earliest epoch of observations is -7 days, and it shows no evidence for HVFs in any of its spectra. Whether the lack of HVFs is related to the presence of carbon or is simply due to the rapid decline rate is unclear. It is worth noting that one of the strongest HVF SNe Ia, SN 2005cf, was also highlighted by Thomas et al. (2011) for having a very clear carbon absorption feature in its early spectra (before about -7 days). Carbon is presumed to originate from the surface of the exploding WD, and it is possible that HVFs could also arise from this same physical location. Thus, we believe that the relationship between unburned carbon and HVFs is a topic worthy of further exploration. Since both spectroscopic behaviours are strongest at earliest epochs, this underscores the need for timely discovery and classification of young SNe Ia.

SN 2004eo. This rapidly declining ($\Delta m_{15}(B) = 1.46$ mag) SN Ia may be at the very faint end of the distribution of normal SNe Ia (Pastorello et al. 2007). Interestingly, SN 2004eo shows a fairly strong Ca II NIR triplet HVF ($R_{\rm HVF} \approx 1$) in its first epoch (-11 days), which declines in strength very slowly. We note here that in the final two epochs (-3 and $+2$ days), the fit to the HVF may be influenced by the weak S II λ8315 line. This feature was also evident in SN 2011fe spectra starting at around -4 days, but due to the high S/N of those spectra fitting of that feature as an HVF of Ca II NIR triplet resulted in a poor χ^2, meaning that for SN 2011fe the profile fits were not affected by this line. For the medium-S/N spectra of SN 2004eo this S II line is more problematic, and we can see that the profile was fitted as an unnaturally strong HVF with the photospheric Ca II NIR triplet having a lower velocity than the Si II λ6355 line (which was generally not the case for the Ca II NIR triplet profiles that were well fit). Thus, for the last two epochs here we suspect the true $R_{\rm HVF}$ value to be closer to 0. This underscores the importance of also calculating the model-independent absorption-weighted velocities: in this quantity we find a leveling off near maximum light, similar to SN 2011fe, consistent with the hypothesis that HVFs in SN 2004eo have actually faded by maximum light. At the very least, the clear presence of HVFs in the earliest epochs (-11 and -7 days) may point to the ubiquity of HVFs in all normal SNe Ia.

SN 1999by and SN 2005bl. These extremely rapidly declining SNe Ia ($\Delta m_{15}(B) = 1.90$ and 1.93 mag for SN 1999by and SN 2005bl, respectively) are members of the subclass of peculiar SNe Ia spectroscopically similar to the subluminous SN 1991bg (Filippenko et al. 1992; Leibundgut et al. 1993). These SNe have the earliest spectra (-4 and -6 days) of any members of the subclass, but show no evidence for HVFs in any of their spectra. This is unsurprising given the absence of HVFs by this epoch in more-

slowly declining SNe Ia and the apparent trend of HVF strength with $\Delta m_{15}(B)$. Whether SN 1991bg-like SNe Ia have HVFs at earlier epochs remains to be seen, and requires earlier detections of these very subluminous SNe.

Using a sample of SNe Ia spanning decline rates from $\Delta m_{15}(B)= 0.97$ mag (SN 2003kf; Hicken et al. 2009) to $\Delta m_{15}(B)= 1.28$ mag (SN 2002er; Ganeshalingam et al. 2010), Mazzali et al. (2005b) found that HVFs were evident in their entire sample of SN Ia spectra taken about a week before maximum light. We confirm this behaviour here for an extended range of $\Delta m_{15}(B)$ (0.80 mag for SN 2012fr to 1.46 mag for SN 2004eo), and echo the suggestion by Mazzali et al. (2005b) that HVFs appear to be a ubiquitous feature of normal SNe Ia which are uniformly stronger at earlier epochs.

However, we find that the pre-maximum HVF evolution does not follow a consistent pattern among all SNe Ia. A consequence of this is that the relative ranking of HVF strength in a sample of SNe Ia at maximum light is not always preserved at very early epochs. Thus, a larger set of pre-maximum SN Ia spectra appears necessary to fully categorise this behaviour and define the best metric(s) to describe the HVF strength of a given SN Ia. Another key result is that several SNe Ia showing no HVFs at maximum light (specifically the high-$v_{\rm Si}$ SN 2009ig and the moderately fast-declining SN 2004eo) *do* exhibit HVFs at earlier epochs. Again, this suggests that the HVF strength at maximum light is not a comprehensive metric of HVF strengths in SNe Ia, as those which are HVF-free at maximum light may have some diversity at earlier epochs when the HVF strength is nonzero.

5 DISCUSSION AND CONCLUSIONS

In this work we conducted an investigation of HVFs in the maximum-light spectra of a sample of 58 SNe Ia, as well as HVFs at all pre-maximum-light epochs in several SNe Ia having extensive spectral time series. Specifically, we focused on HVFs in the Ca II NIR triplet feature, using epochs where the Si II λ6355 line was clean of HVFs to help define the photospheric velocity profile. We quantified the HVF strength with two metrics: (1) the pEW ratio of the Ca II NIR triplet HVF to the photospheric absorption component, as measured from a fit to the Ca II NIR triplet velocity profile; and (2) the difference in the absorption-weighted velocity of the Si II λ6355 line and the Ca II NIR triplet. The first method provided a physically meaningful but model-dependent measurement of the HVF strength, while the second allowed for agnostic measurement of the mean velocity of the Si II λ6355 line and Ca II NIR triplet absorption profiles. From our analysis, we found important trends in HVF behaviour, as follows.

- SNe Ia with rapidly declining light curves ($\Delta m_{15}(B) \geq 1.4$ mag) have consistently no HVFs at maximum light, and for normal SNe Ia the average HVF strength tends to increase with decreasing light-curve decline rate.
- SNe Ia with a high silicon velocity ($v_{\rm Si}\geq$ 12,000 km s^{-1}) at maximum light (i.e., the "HV" subclass identified by Wang et al. 2009a) also show no evidence for HVFs at maximum light. A trend of HVF strength with $v_{\rm Si}$ is also evident, but it is weaker than the trend with $\Delta m_{15}(B)$.
- The pre-maximum-light evolution of HVFs exhibits significant diversity, with the rate of HVF fading showing no clear dependence on the overall HVF strength, $\Delta m_{15}(B)$, or $v_{\rm Si}$.
- Some SNe Ia which show weak or no HVFs at maximum light (specifically, the high-$v_{\rm Si}$ SN 2009ig and the fast-declining SN 2004eo) were found to have HVFs in very early spectra.

The original goal of this project was to examine the influence of HVF Ca on the Ca II H&K line complex, to confirm whether the stretch dependence of this line complex noted by Maguire et al. (2012) was caused by HVF Ca as those authors proposed, or whether it could be due primarily to the Si II λ3858 line as posited by Foley (2012). We found that although the wavelength-space degeneracy of HVF Ca II H&K and Si II λ3858 prevented a direct decoupling of these lines in the Ca II H&K line complex, the Ca II NIR triplet provided a clean independent measurement of the influence of HVFs. Our finding that HVFs in the Ca II NIR triplet are stronger in more-slowly declining (i.e., higher "stretch") SNe Ia supports the interpretation of Maguire et al. (2012). However, the Si II λ3858 line does appear to impact the Ca II H&K line complex in nearly all cases, as evidenced by the difference in absorption-weighted velocities for Ca II H&K compared to the Ca II NIR triplet, lending some credence to the argument of Foley (2012) that Si II λ3858 affects the Ca II H&K line profile.

The origin of the HVFs remains unknown, but numerous hypotheses have been presented (see Section 1). Our findings provide important observations of the behaviour of HVFs in relation to $\Delta m_{15}(B)$ and $v_{\rm Si}$ which offer constraints on possible models of their origin. While the HVFs themselves are identified by their distinct absorption profiles, the HVF material could potentially cause some smooth alteration of the full SN spectral energy distribution not easily identifiable from SN spectra, which in turn could impact the degree to which SN Ia luminosities can be standardized. We confirmed the findings of previous authors that the strength of HVFs is consistently greater at earlier epochs. This underscores the need for the earliest possible spectroscopic observations of SNe Ia in order to further inspect this important facet of their behaviour.

Acknowledgements: We thank Stefan Taubenberger for providing his spectra of SN 2005bl; Jeffrey Silverman for his hard work on the BSNIP sample; the late Weidong Li for his key role in obtaining the KAIT light curves published by LOSS (Ganeshalingam et al. 2010); Stuart Sim, Richard Scalzo, Brad Tucker, and Ryan Foley for helpful discussions; and the Lick Observatory staff for their assistance with the observations. We also thank the anonymous referee for thoughtful and constructive comments. This research was conducted by the Australian Research Council Centre of Excellence for All-sky Astrophysics (CAASTRO), through project number CE110001020. B.P.S. acknowledges support from the Australian Research Council Laureate Fellowship Grant LF0992131. A.V.F. is grateful for the generous financial support of NSF grant AST-1211916, the TABASGO Foundation, and the Christopher R. Redlich Fund. KAIT has been funded by donations from Sun Microsystems, Inc., the Hewlett-Packard Company, AutoScope Corporation, Lick Observatory, the NSF, the University of California, the Sylvia & Jim Katzman Foundation, the Christopher R. Redlich Fund, the Richard and Rhoda Goldman Fund, and the TABASGO Foundation. This research has made use of NASA's Astrophysics Data System (ADS).

REFERENCES

Benetti, S., et al. 2005, ApJ, 623, 1011
Blondin, S., Dessart, L., Hillier, D. J., & Khokhlov, A. M. 2013, MNRAS, 429, 2127
Blondin, S., et al. 2012, AJ, 143, 126

Branch, D., Dang, L. C., & Baron, E. 2009, PASP, 121, 238
Burns, C. R., et al. 2011, AJ, 141, 19
Childress, M. J., et al. 2013, ApJ, 770, 29
Chotard, N., et al. 2011, A&A, 529, L4
Contreras, C., et al. 2010, AJ, 139, 519
Filippenko, A. V., Li, W. D., Treffers, R. R., & Modjaz, M. 2001, in Astronomical Society of the Pacific Conference Series, Vol. 246, IAU Colloq. 183: Small Telescope Astronomy on Global Scales, ed. B. Paczynski, W.-P. Chen, & C. Lemme, 121
Filippenko, A. V., et al. 1992, AJ, 104, 1543
Foley, R. J. 2012, arXiv:1212.6261
Foley, R. J., & Kasen, D. 2011, ApJ, 729, 55
Foley, R. J., Sanders, N. E., & Kirshner, R. P. 2011, ApJ, 742, 89
Foley, R. J., et al. 2012, ApJ, 744, 38
Ganeshalingam, M., Li, W., & Filippenko, A. V. 2011, MNRAS, 416, 2607
Ganeshalingam, M., et al. 2010, ApJS, 190, 418
Garavini, G., et al. 2007, A&A, 471, 527
Garnavich, P. M., et al. 2004, ApJ, 613, 1120
Gerardy, C. L., et al. 2004, ApJ, 607, 391
Hachinger, S., Mazzali, P. A., Tanaka, M., Hillebrandt, W., & Benetti, S. 2008, MNRAS, 389, 1087
Hicken, M., et al. 2009, ApJ, 700, 331
Hoeflich, P., & Khokhlov, A. 1996, ApJ, 457, 500
Jha, S., Riess, A. G., & Kirshner, R. P. 2007, ApJ, 659, 122
Kelly, P. L., Hicken, M., Burke, D. L., Mandel, K. S., & Kirshner, R. P. 2010, ApJ, 715, 743
Leibundgut, B., et al. 1993, AJ, 105, 301
Maguire, K., et al. 2012, MNRAS, 426, 2359
Marion, G. H., et al. 2013, arxiv:1302.3537
Mazzali, P. A., Benetti, S., Stehle, M., Branch, D., Deng, J., Maeda, K., Nomoto, K., & Hamuy, M. 2005a, MNRAS, 357, 200
Mazzali, P. A., Nomoto, K., Cappellaro, E., Nakamura, T., Umeda, H., & Iwamoto, K. 2001, ApJ, 547, 988
Mazzali, P. A., Röpke, F. K., Benetti, S., & Hillebrandt, W. 2007, Science, 315, 825
Mazzali, P. A., et al. 2005b, ApJL, 623, L37
Miller, J. S., & Stone, R. P. S. 1993, Lick Obs. Tech. Rep. 66 (Santa Cruz: Lick Obs.)
Neill, J. D., et al. 2009, ApJ, 707, 1449
Nugent, P., Phillips, M., Baron, E., Branch, D., & Hauschildt, P. 1995, ApJL, 455, L147
Parrent, J. T., et al. 2012, ApJL, 752, L26
Pastorello, A., et al. 2007, MNRAS, 377, 1531
Patat, F., Benetti, S., Cappellaro, E., Danziger, I. J., della Valle, M., Mazzali, P. A., & Turatto, M. 1996, MNRAS, 278, 111
Pereira, R., et al. 2013, A&A, 554, A27
Perlmutter, S., et al. 1999, ApJ, 517, 565
Phillips, M. M. 1993, ApJL, 413, L105
Pinto, P. A., & Eastman, R. G. 2000, ApJ, 530, 757
Riess, A. G., Press, W. H., & Kirshner, R. P. 1996, ApJ, 473, 88
Riess, A. G., et al. 1998, AJ, 116, 1009
Seitenzahl, I. R., et al. 2013, MNRAS, 429, 1156
Silverman, J. M., Kong, J. J., & Filippenko, A. V. 2012a, MNRAS, 425, 1819
Silverman, J. M., et al. 2012b, MNRAS, 425, 1789
Sim, S. A., Röpke, F. K., Hillebrandt, W., Kromer, M., Pakmor, R., Fink, M., Ruiter, A. J., & Seitenzahl, I. R. 2010, ApJL, 714, L52
Smith, M., et al. 2012, ApJ, 755, 61
Stritzinger, M. D., et al. 2011, AJ, 142, 156
Sullivan, M., et al. 2011, ApJ, 737, 102
Tanaka, M., Mazzali, P. A., Maeda, K., & Nomoto, K. 2006, ApJ, 645, 470
Tanaka, M., et al. 2008, ApJ, 677, 448
Taubenberger, S., et al. 2008, MNRAS, 385, 75
Thomas, R. C., et al. 2007, ApJL, 654, L53
—. 2011, ApJ, 743, 27
van Rossum, D. R. 2012, arXiv:1208.3781
Wang, X., Wang, L., Filippenko, A. V., Zhang, T., & Zhao, X. 2013, Science, 340, 170
Wang, X., et al. 2009a, ApJL, 699, L139
—. 2009b, ApJ, 697, 380
Yaron, O., & Gal-Yam, A. 2012, PASP, 124, 668